ROBUST AERODYNAMIC DESIGN OPTIMISATION OF MORPHING AEROFOIL/WING USING DISTRIBUTED MOGA

D.S. Lee[*,**], L. F. Gonzalez[**], J. Periaux[*,***], E. Onate[*,***]**
*** Centre Internacional de Metodes Numerics en Enginyeria (CIMNE), Barcelona 08034, Spain**
**** Australian Research Centre for Aerospace Automation (ARCAA), Queensland University of Technology (QUT), Brisbane, QLD 4001, Australia**
***** Universitat Politecnica de Catalunya, Campus Norte UPC, Barcelona 08034, Spain**
****** Deloitte Analytics – Deloitte Consulting LLC, Seoul, Korea**

Keywords: *Robust/Uncertainty Design, Multi-Objective Genetic Algorithms (MOGA), Parallel Computing, Morphing Wing*

Abstract

In this paper, the shape design optimisation using morphing aerofoil/wing techniques, namely the leading and/or trailing edge deformation of a natural laminar flow RAE 5243 aerofoil is investigated to reduce transonic drag without taking into account of the piezo actuator mechanism. Two applications using a Multi-Objective Genetic Algorithm (MOGA) coupled with Euler and boundary analyser (MSES) are considered: the first example minimises the total drag with a lift constraint by optimising both the trailing edge actuator position and trailing edge deformation angle at a constant transonic Mach number ($M_\infty = 0.75$) and boundary layer transition position (x_{tr} = 45%c). The second example consists of finding reliable designs that produce lower mean total drag (μCd) and drag sensitivity (σCd) at different uncertainty flight conditions based on statistical information.

Numerical results illustrate how the solution quality in terms of mean drag and its sensitivity can be improved using MOGA software coupled with a robust design approach taking account of uncertainties (lift and boundary transition positions) and also how transonic flow over aerofoil/wing can be controlled to the best advantage using morphing techniques.

1 Introduction

Civil and military aviation are now exploring the implementation of morphing technology consists to adapting a suitable shape with repect to flight conditions and to improve of aerodynamic efficiency (L/D) and the total drag (Cd_{Total}) reduction. Used in class of Active Flow Control (AFC) devices, morphing technologies can help significantly to control transonic flow over the wing and consequently reduce Direct Operating Cost (DOC) by lowering total drag [1, 2].

In this paper, a class of morphing technologies Leading and/or Trailing Edge Deformation (LTED) allowing deformation of a natural laminar flow aerofoil RAE 5243 [3] is investigated to reduce transonic drag without taking into account details of piezo actuator mechanism. LTED technology is one of the applicable morphing techniques to the aviation due to simple mechanism using either piezo or hydraulic actuator, and less modification compared to other morphing techniques, which can change more than 50% of total shape. Despite LTED technology operates with a simple mechanism, it is nevertheless very sensitive to possible uncertain flow conditions during flight especially for lift coefficient (Cl) numbers varying in the interval of [0.458:0.648] and for boundary layer transition positions (x_{tr})

in the interval of [0:50%c]. These uncertainty parameters are directly responsible of the position and strength of the shock on the suction/pressure side of the wing. It is therefore important to find suitable and reliable actuator positions and deformation angles using robust design methods [4, -6].

The paper investigates the shape design optimisation for morphing aerofoil/wing to reduce the total drag during cruise conditions using Multi-Objective Genetic Algorithm (MOGA). For running the MOGA software, Robust Multi-objective Optimisation Platform (RMOP) developed at CIMNE is used. RMOP is capable to perform High Performance Computing (HPC) using Distributed MOGA (DMOGA) [7]. In this paper, two applications are considered: the first application minimises the total drag with a lift constraint by adapting both the TE actuator position and TE deformation angle at fixed Mach number (M_∞ = 0.75) and boundary layer transition position (x_{tr} = 45%c). The second application captures reliable designs (TE actuator position and deformation angle) that produce lower mean total drag (μCd) and drag sensitivity (σCd) at different flight conditions representing uncertainties occurring during flight conditions (μCl = 0.5558, σCl = 0.0611 and μx_{tr} = 0.2565, σx_{tr} = 0.1604). Numerical results obtained from two practical optimisations are compared in terms of drag quality (mean drag and its sensitivity) in the design.

The rest of paper organized as follows; Section 2 introduces the MOGA used in this paper. Section 3 describes the Euler and boundary analyser. Section 4 details two applications for morphing aerofoil/wing design optimization. Section 5 concludes overall numerical results and presents ongoing research avenues.

2 Methodology

2.1 Robust Multi-objective Optimisation Platform (RMOP)

RMOP is a computational intelligence framework which is a collection of population based algorithms including Genetic Algorithm (GA) and Particle Swarm Optimisation (PSO) [8 -10]. As shown in Figure 1, RMOP consists of the eight modules;

- EVAU (Evaluation Unit) is a module for evaluation and collecting results from analysis tools.
- IOPU (In/Output Unit) is a module for handling input, output data and also plotting convergence history, initial random population(s) (with/without buffer population), total populations, and Pareto optimal front.
- IRPU (Initial Random Population Unit) is an initial random population module.
- MEAU (Memory Allocation Unit) is a module for allocating/dis-allocating memory for population(s) and also to provide parallel/distributed computation.
- NDOU (Non-Dominated Optimal Unit) is a module for computing Pareto-tournament, non-dominated sorting solutions.
- RANU (Random Number Unit) is a module for generating pseudo random number module.
- SSOU (Searching/Selection Objective Unit) is a searching module; selection, mutation, crossover for GA and also it produces velocity, positioning module for PSO.

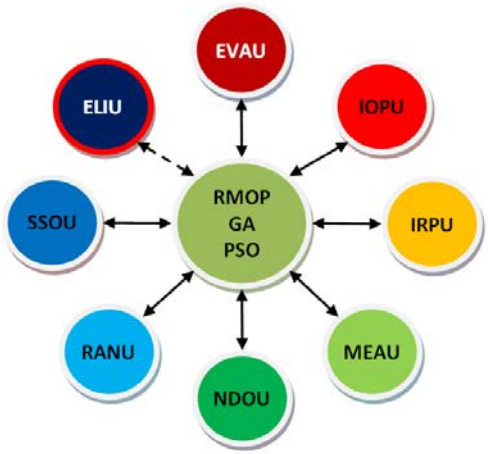

Fig. 1. Robust Multi-objective Optimisation Platform.

In this paper, RMOP uses GA searching method incorporating with a parallel computing module;

MEAU for high performance computing (denoted as DMOGA).

2.2 Parallel/Distributed Computation

RMOP with OpenMP [11] can provide a High Performance Computing environment; the number of CPU cores defined by the user will handle the same number of individuals (member of population) of GA or PSO at the same time. In other words, the total numbers of tasks are distributed to available CPUs to evaluate a design model with CFD analysis tool during the optimisation as shown in Figure 2. A parallel computation during the optimisation can improve a physical performance of MOEA.

In this paper, distributed Multi-Objective GA (DMOGA) uses ten cores simultaneously while RMOGA uses the default value (1) in a Dell PowerEdge 6850 (Intel(R) Xeon(TM) CPU 16 × 3.20GHz and 32GB RAM) machine.

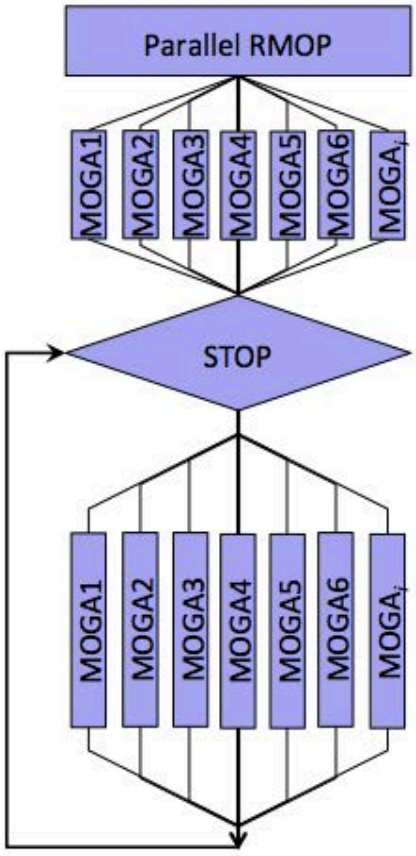

Fig. 2. Ditributed/Parallel Computation in RMOP.

3 Aerodynamic Analysis Tools: MSES (Euler and Boundary)

In this paper, the Euler and Boundary layer aerodynamic analysis MSES software tool written by Drela [12] is used for simulating the flow field around the aerofoils in design problems discussed Section 4. The MSES software is a coupled viscous/inviscid Euler method for the analysis and design of multi-element/single-element aerofoils for a wide range of Mach and Reynolds numbers. It has capabilities to predict flows with transitional separation bubbles, shock waves, trailing edge and shock-induced separation. Transition can be forced or predicted as part of the flow calculation. MSES automatically adjusts angle of attack (α) to obtain a predefined lift coefficient (C_l), the angle of attack of the aerofoil is adapted.

A validation test case is conducted at the flight conditions; Mach number (M_∞) = 0.729, angle of attack (α) = 2.31° and Reynolds number (Re) = 6.5×10^6. Figure 3 shows the mesh (36 × 213) obtained by MSES that will be used for code validation and during the optimisation (Section 5). Figure 4 compares the results obtained by MSES and wind tunnel experimental data [13]. It can be seen that there is a good agreement between Cp distributions obtained by MSES and wind tunnel data.

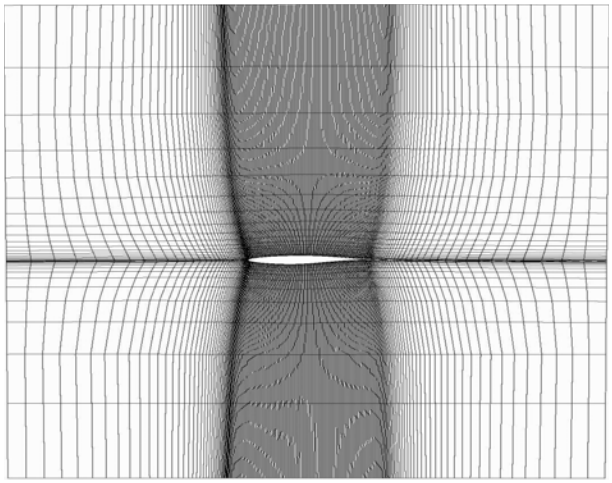

Fig. 3. RAE 2822 aerofoil mesh obtained by MSES.

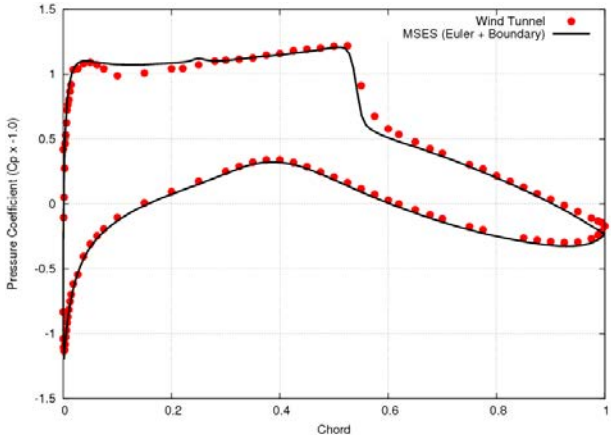

Fig. 4. Comparison of *Cp* distributions obtained by MSES (line) and wind tunnel experimental data (dots).

4 Morphing Aerofoil Design Optimisation using Distributed MOGA

4.1 Parameterization of Morphing Aerofoil/Wing; Leading and Trailing Edge Deformation (LTED)

The Leading and Trailing Edge Deformation (LTED) morphing technique can be defined by four control parameters as shown in Figure 5; leading edge actuator position (x_{LE}), trailing edge actuator position (x_{TE}), deformation angle for leading edge (θ_{LE}), and deformation angle for trailing edge (θ_{TE}).

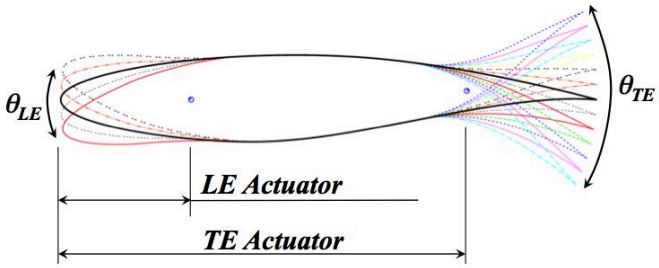

Fig. 5. Control parameters for morphing technique at fixed leading and trailing edge actuator positions.

Deformation angles for follow the right-hand rule. Figure 6 shows a morphing technique mechanism consisting of four steps;

- Step 1: Find actuator positions for leading and trailing edges; x_{LE}, y_{LE}, x_{TE}, y_{TE} (marked as green crosses),
- Step 2: Deform leading edge by θ_{LE},
- Step 3: Deform trailing edge by θ_{TE},
- Step 4: Smooth sharp joint (marked as red circles shown in Figure 4) using Bezier Spline Curves; BSC1, BSC2, BSC3, and BSC4.

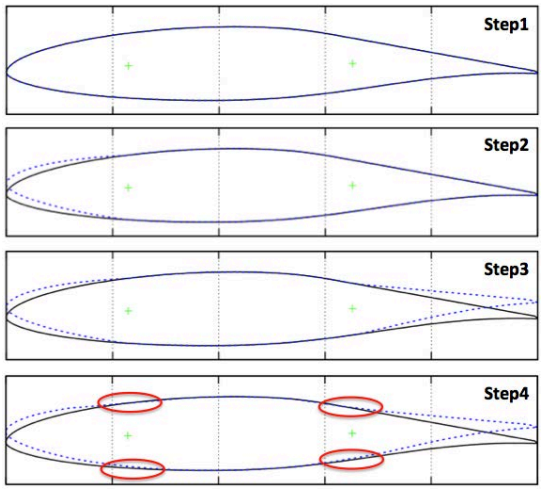

Fig. 6. LTED morphing mechanism.

If the problem considers only trailing edge deformation then the morphing mechanism will go through Step1 → Step3 → Step4.

4.2 Formulation of Design Problem

For the baseline design, a natural laminar flow aerofoil RAE 5243 is selected as shown in Figure 7. The baseline design has a maximum thickness ratio (*t/c*) of 0.14 at 41% of the chord and the maximum camber of 0.018 at 54 % of the chord.

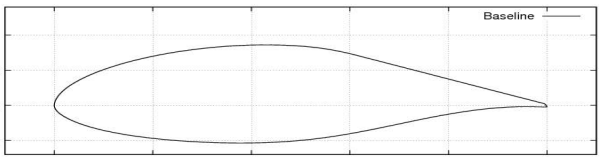

Fig. 7. Baseline design (RAE 5243) geometry (Note: max *t/c* = 0.14 at 41%c and max camber = 0.018 at 54%c).

In the following Sections 4.3 and 4.4, the shape of the baseline design will be adapted to control the transonic flow especially to maximise the lift to drag ratio with a lift coefficient constraint.

4.3 Transonic Morphing Aerofoil/Wing Design Optimisation

Problem Definition

This test case considers a single objective morphing aerofoil design optimisation to minimise the total drag at a constant lift coefficient. In other words, the objective is to maximise the lift to drag ratio (L/D) so the aircraft can extend flight range. The flow conditions are $M_\infty = 0.75$, $Cl_\infty = 0.45819$ and Re $= 19.0 \times 10^6$. The fitness function for DMOGA is shown in Equation (1).

$$f(x_{TE}, \theta_{TE}) = min(Cd_{Total}) \quad (1)$$
$$= min(Cdv + Cdw)$$

Subject to

$$Cl_{min} = 0.45819$$

where $Cd_{Total} = Cd_{Visous} + Cd_{Wave}$.

The constant lift coefficient is calculated using Equation (2) which represents the minimum lift coefficient of the aircraft in level flight.

$$Cl_{min} = 2W/\rho V^2 S \quad (2)$$

where; W is the weight force ($m \times g$) of the aircraft: mass m = 77,564 kg and acceleration of gravity g = 9.81 m/s^2, ρ is the air density at 35,000 ft: ρ = 0.41 kg/s^3, S is the wing area: S = 124.58 m^2.

Design Variables

The design variable bounds for trailing edge deformation (TED) are illustrated in Table 1. All Bezier Spline Curves (BSC) shown in Figure 4; BSC3 and BSC4 have a constant length of 20% of chord length. BSC3 and BSC4 have the same x-axis Bezier control points (starting, peak, finishing points). So two design parameters are considered in total.

Table 1. Design Bounds for Morphing Aerofoil/Wing using trailing edge deformation.

DVs	x_{TE}	θ_{TE}
Lower Bound	65.0	- 5.0°
Upper Bound	75.0	+ 5.0°

Note: DVs represents design variables. x_{TE} is in the baseline chord length (%c) [0:100] and deformation angle follows right-hand rule.

Numerical Results

The algorithm was allowed to run for 1 hour (as time stopping criterion) and for 6,020 function evaluations. Convergence occurred after 617 function evaluations as shown in Figure 8.

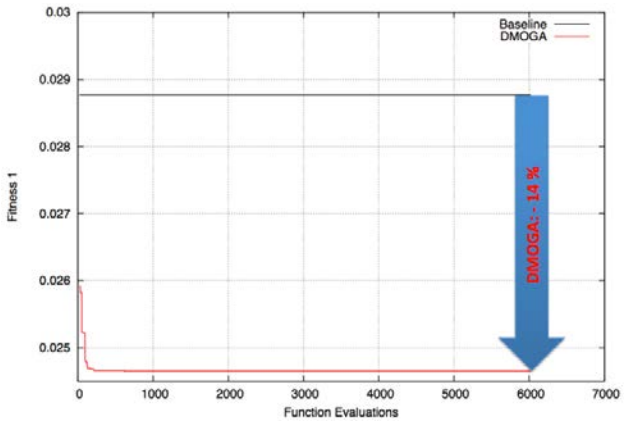

Fig. 8. Convergence history obtained by DMOGA.

Table 2 compares the aerodynamic characteristics obtained by the baseline design (RAE 5243) and the optimal solution obtained by DMOGA. Even though applying optimal morphing configuration slightly increases the wave drag, the viscous drag is reduced by 27.2 % which results in improving the lift to drag ratio by 16.4 %.

Table 2. Aerodynamic Characteristics obtained by DMOGA.

Aerofoil	*Cdv*	*Cdw*	*L/D*
Baseline	0.0213	0.0074	15.93
DMOGA	0.0155 (- 27.2%)	0.0088 (+ 19.0%)	18.55 (+ 16.4%)

Note: *Cdv* and *Cdw* represent viscous and wave drag, and the sum of them is the total drag of aerofoil.

Table 3 describes the optimal morphing (trailing deformation) configurations obtained by DMOGA. Figure 9 compares the geometry of the baseline design and the baseline with the optimal morphing configurations. The optimal solution has the same maximum thickness ratio (t/c) of 0.14 as the baseline design at 41% of the chord, while the maximum camber is lowered by 1.2%c (max camber = 0.0066 at 29.0%c).

Table 3. Optimal Morphing Configurations obtained by DMOGA.

Variables	x_{TE} (%c)	θ_{TE}
DMOGA	65.04	- 4.5195°

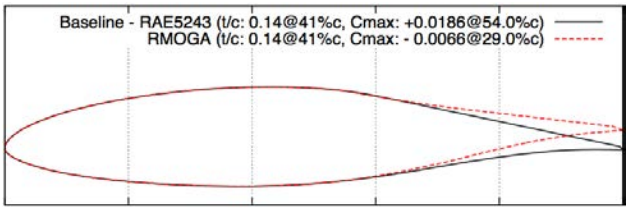

Fig. 9. Comparison of geometry obtained by Baseline design and the optimal morphing configurations obtained by DMOGA (max t/c = 0.14 at 41%c and max camber = -0.0066 at 29.0%c).

Figure 10 compares the lift coefficient sweep obtained by the baseline design and the optimal morphing configuration at range of [0.1:0.8] with M_∞ = 0.75 and Re = 19.0 × 10^6. Even though the optimal morphing solution produces lower total drag when the lift coefficient is lower than 0.55 (Fig. 10. top), it produces higher wave drag when the lift coefficient is higher than 0.38 (Fig. 10. bottom).

Therefore it is necessary to optimise the morphing configuration with uncertainty parameters including lift coefficients and boundary transition positions (x_{tr}). Both uncertainty parameters are directly affecting the strength and position of shock.

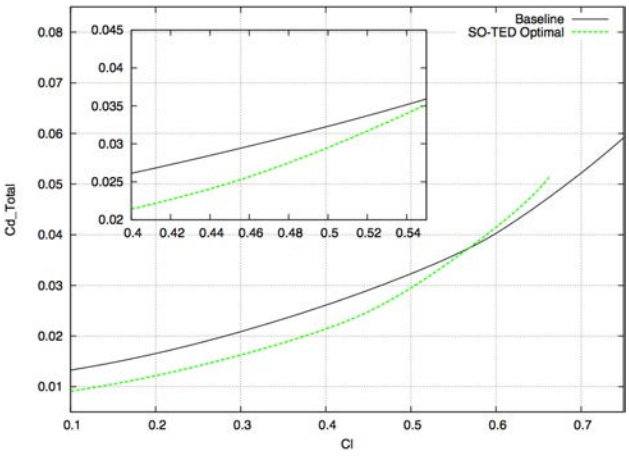

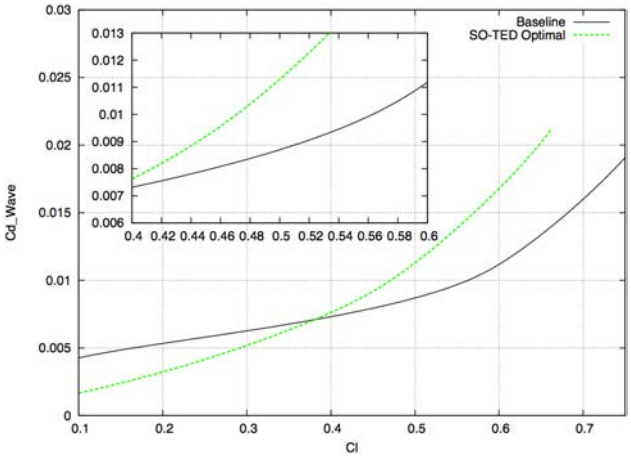

Fig. 10. Cd_{Total} vs. Cl (top) and Cd_{Wave} vs. Cl (bottom) sweep obtained by the baseline design and the optimal morphing configuration at range of [0.1:0.75] with M_∞ = 0.75, Re = 19.0 × 10^6 and μx_{tr} = 45%c.

4.4 Robust Transonic Morphing Aerofoil/Wing Design Optimisation

Problem Definition

This test case considers a robust multi-objective morphing aerofoil/wing design optimisation on the RAE 5243 aerofoil to minimize the average and standard deviation of the total drag (μCd_{Total}, σCd_{Total}) at flow conditions M_∞ = 0.75 and Re = 19.0 × 10^6.

Introducing uncertainties on operating flow conditions, two sets of ten values of lift coefficient (Cl) and then of boundary layer transition positions (x_{tr}) are considered. Both uncertainty parameters; Cl and x_{tr} can be statistically defined as μCl = 0.5558, σCl = 0.0611 in a range of $Cl_\infty \in$ [0.458, 0.648], and μx_{tr} = 0.2565, σx_{tr} = 0.1604 in a range of $x_{tr\infty} \in$ [0.0, 50.0%c]. The candidate morphing aerofoil/wing model will be evaluated at hundred flight conditions (10 x_{tr} × 10 C_l). The robust fitness functions are shown in equations (3) and (4) respectively.

$$f_1 = \min\left(\mu Cd_{Total}\right) = \frac{1}{n \times m}\sum_{i=1}^{n}\sum_{j=1}^{m} Cd_{Total_{ij}} \qquad (3)$$

$$f_2 = \min\left(\sigma Cd_{Total}\right) = \sqrt{\frac{1}{n \times m - 1}\sum_{i=1}^{n}\sum_{j=1}^{m}\left(Cd_{Total_{ij}} - \mu Cd_{Total}\right)^2} \quad (4)$$

where n and m represent the number of boundary layer transition positions and C_l conditions repectively.

Design Variables

The design variable lower and upper bounds for morphing geometry via leading and trailing edge deformation are illustrated in Table 4. The length of all Bezier Spline Curves (BSC shown in Figure 6); BSC1, BSC2, BSC3, and BSC4, are selected as additional design parameters to find more sophisticated morphing shape. Finally eight design variables are considered in total.

Table 4. Design Bounds for Morphing Aerofoil/Wing using trailing edge deformation.

LDVs	x_{LE}	θ_{LE}	L_{BSC1}	L_{BSC2}
Lower	15.0	- 5.0°	10.0	10.0
Upper	25.0	+ 7.5°	25.0	25.0
TDVs	x_{TE}	θ_{TE}	L_{BSC3}	L_{BSC4}
Lower	65.0	- 10.0°	10.0	10.0
Upper	75.0	+ 5.0°	30.0	30.0

Note: L/TDVs represents leading and trailing edge design variables. x_{LE}, x_{TE} are expressed with respect to in the baseline chord length (%c) [0:100] and deformation angle follows right-hand rule. L_{BSCi} represents the length of the ith BSC (%c).

Numerical Results

The algorithm was allowed to run for 20 hours (a selected time stopping criterion) and for 600 function evaluations. Figure 11 compares Pareto optimal front obtained by DMOGA (denoted as RO-LTED) with the baseline design and the optimal solution obtained in Section 4.3 (denoted as SO-TED). It can be seen that all Pareto optimal solutions in Zone-A dominate the baseline design and the optimal solution; SO-TED (obtained in Section 4.3) in both the mean total drag and total drag standard deviation. In Zone-B, the baseline design dominates the optimal solution obtained in Section 4.3. Pareto members 2 and 3 are selected as a compromised solution and denoted as RO-LTED.

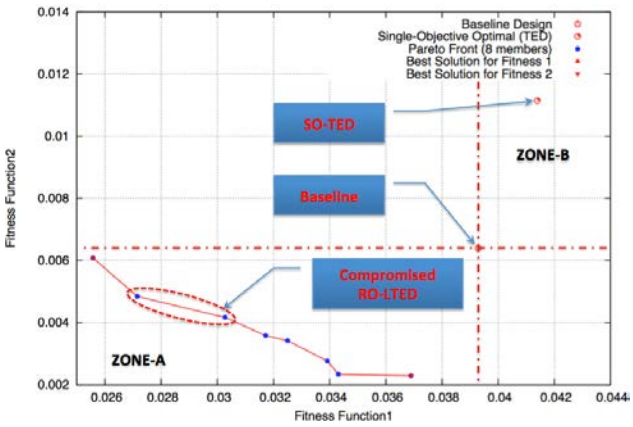

Fig. 11. Pareto optimal front obtained by DMOGA.

Table 5 compares the fitness values obtained by the baseline design, the optimal solutions from Section 4.3 and the Pareto members 1 (Best solution for the objective 1), 2 and 3 (Compromised Solution), and 8 (Best solution for the objective 2).

Table 5. Comparison of Drag Quality.

Aerofoil	μCd	σCd	$\mu L/D$
Baseline	3.93×10^{-2}	6.40×10^{-3}	14.14
Optimal (Section 4.3)	4.14×10^{-2} (+ 5.3%)	11.1×10^{-3} (+ 73.4%)	13.42 (- 5.1%)
DMOGA (BO1-PM1)	2.55×10^{-2} (- 35.1%)	6.07×10^{-3} (- 5.1%)	21.79 (+ 54.1%)
DMOGA (CS-PM2)	***2.71×10^{-2} (- 31.0%)***	***4.84×10^{-3} (- 24.4%)***	***20.51 (+ 45.0%)***
DMOGA (CS-PM3)	***3.02×10^{-2} (- 23.1%)***	***4.16×10^{-3} (- 35.0%)***	***18.40 (+ 30.1%)***
DMOGA (BO2-PM8)	3.68×10^{-2} (- 6.4%)	2.28×10^{-3} (- 64.3%)	15.10 (+ 6.8%)

Note: BOi and PMi represent the best solution of ith objective and the ith Pareto member respectively. CS stands for a Compromised Solution.

It can be seen that the optimal solution obtained in Section 4.3 has higher mean total drag and higher total drag standard deviation by 5.3% and 73% respectively when compared to the baseline design. Even though the best solutions (Pareto members 1 and 8) for objectives 1 and 2

have lower mean total drag and lower total drag standard deviation respectively, one of the compromised solutions Pareto member 2 has lower mean total drag and lower standard deviation of total drag when compared to the baseline design. The mean and standard deviations obtained by the baseline design, single-objective and robust Pareto members can also be compared using Cumulative Distribution Function (CDF) and Probability Density Function (PDF) as shown in Figure 12.

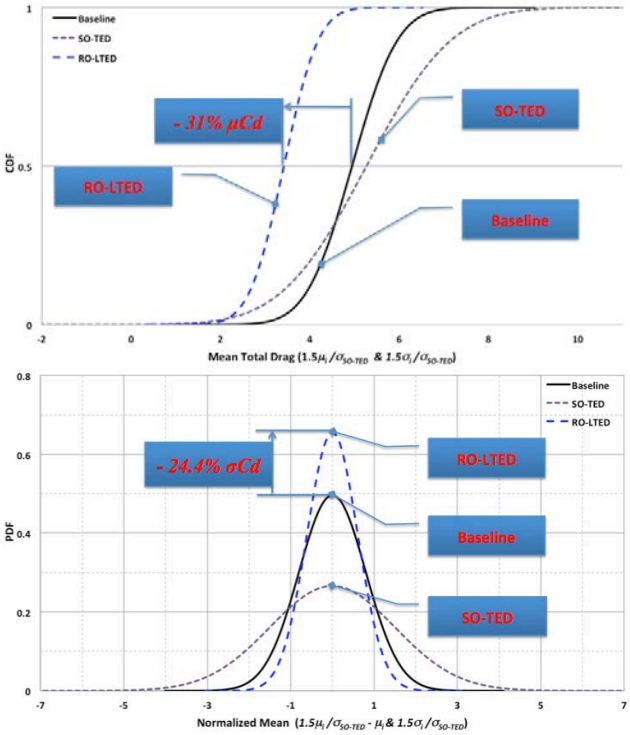

Fig. 12. Mean and standard deviation of total drag comparison using CFD (top) and PDF (bottom).

Figure 12 shows that the robust optimal solution lowers mean total drag by 31% when compared to the baseline design. The standard deviation (sensitivity) can be analysed by evaluating gradient of the lines to the CDF value of 0.5 or 1 (steeper gradient means lower sensitivity). The PDF plotted in Figure 10 (bottom) shows sensitivity comparison between the baseline design, single-objective and robust optimal solutions. It can be seen that the solution (Pareto member 2) obtained by robust design method has lower sensitivity (narrower and taller bell curve). Pareto member 2 obtained by the robust design method reduces the total drag sensitivity by 24% while the optimal solution obtained in Section 4.3 (SO-TED) has higher total drag sensitivity by 73% when compared to the baseline design. In other words, the robust design method has capabilities to produce a set of solutions, which have better performance and sensitivity when compared to the single-objective optimisation method.

The optimal morphing configurations (Pareto member 2) for robust design optimisation are described in Table 6. Figure 13 compares the geometry of the baseline design and the baseline with the red-dot geometry of optimal morphing configurations. The optimal solution has the same maximum thickness ratio (t/c) of 0.14 as the baseline design at 41% of the chord, while the maximum camber is lowered by 0.6%c (max camber = - 0.006 at 17.4%c).

Table 6. Optimal Morphing (LTED) Configurations for the robust design optimisation.

LDVs	x_{LE}	θ_{LE}	L_{BSC1}	L_{BSC2}
Optimal	17.2	+ 6.5°	13.4	10.8
TDVs	x_{TE}	θ_{TE}	L_{BSC3}	L_{BSC4}
Optimal	73.0	- 3.0°	21.5	25.3

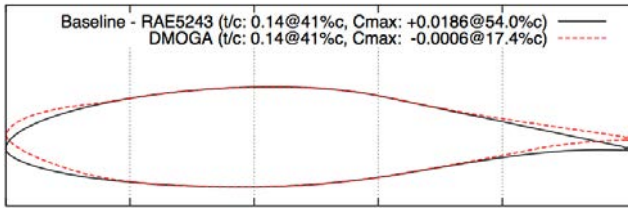

Fig. 13. Baseline design with the optimal morphing configurations obtained by DMOGA (max t/c = 0.14 at 41%c and max camber = - 0.006 at 17.4%c).

Table 7 compares the aerodynamic characteristics obtained by the baseline design (RAE 5243) and the robust optimal solution (Pareto member 2) obtained by DMOGA at the flight conditions of $M_\infty = 0.75$, $Cl_\infty = 0.5558$, x_{tr} = 25.65%c and Re = 19.0×10^6. The robust optimal solution reduces the viscous and wave drag by 43% and 26% respectively that results in improving the lift to drag ratio (L/D) by 66%.

Table 7. Aerodynamic Characteristics obtained by the baseline design and robust solution (Pareto member 2).

Aerofoil	*Cdv*	*Cdw*	*L/D*
Baseline	0.0304	0.0078	14.498
DMOGA	0.0172	0.0058	24.070
ParetoM2	(- 43.4%)	(- 25.6%)	(+ 66.0%)

Note: *Cdv* and *Cdw* represent viscous and wave drag, and Cd_{Total}, the sum of them, denotes the total drag of aerofoil.

Figure 14 shows pressure coefficient contours obtained by the baseline design and the robust optimal solution (Pareto member 2) at flight conditions of $M_\infty = 0.75$, $Cl_\infty = 0.5558$, x_{tr} = 25.65%c and Re = 19.0×10^6. It can be seen that the position of shock is delayed and its strength is reduced.

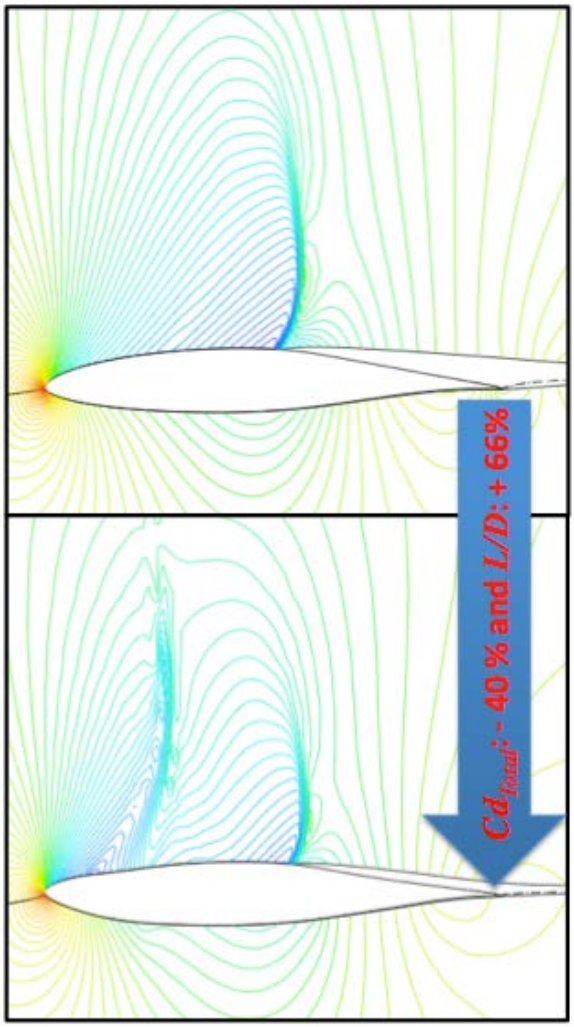

Fig. 14. *Pressure* (C_P) contours obtained by the baseline design and the robust optimal solution (Pareto member 2) at the flight conditions of M_∞ = 0.75, Cl_∞ = 0.5558, x_{tr} = 25.65%c and Re = 19.0×10^6.

Figure 15 compares the lift coefficient sweep obtained by the baseline design, the optimal solution obtained in Section 4.3 (SO-TED) and the robust optimal morphing configuration (Pareto member 2: RO-LTED) at range of $Cl_\infty \in [0.1{:}0.7]$ with $M_\infty = 0.75$, x_{tr} = 25.65%c and $Re = 19.0 \times 10^6$. It can be seen that the optimal solution obtained in Section 4.3 produce lower total drag when *Cl* is lower than 5.5 while the robust optimal solution produces lower total drag for all *Cl* values.

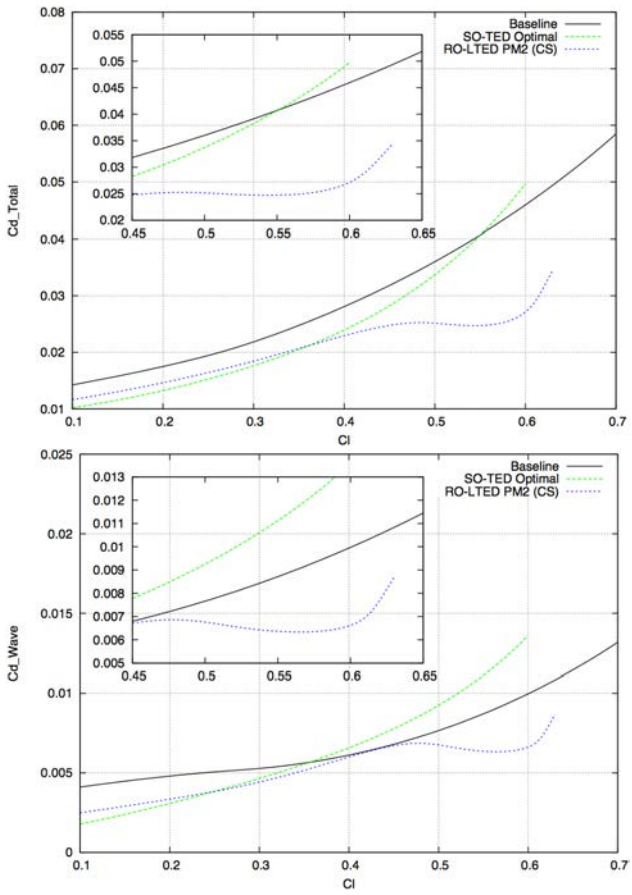

Fig. 15. Cd_{Total} vs. *Cl* (top) and Cd_{Wave} vs. *Cl* (bottom) sweep obtained by the baseline design and the optimal morphing configuration at *Cl* range of [0.1:0.7] with $M_\infty = 0.75$, $Re = 19.0 \times 10^6$ and μx_{tr} = 25.65%c.

Figure 16 compares the lift coefficient sweep obtained by the baseline design, the optimal solution obtained in Section 4.3 (SO-TED) and the robust optimal morphing

configuration (Pareto member 2) at range of $M_\infty \in [0.5{:}0.75]$ with $\mu Cl = 0.5558$, $\mu x_{tr} = 25.65\%c$ and $Re = 19.0 \times 10^6$. It can be seen that the optimal solution obtained in Section 4.3 produce higher total drag when Mach number is higher than 0.748 when compared to the baseline design while the robust optimal solution produces lower total drag when Mach number is higher than 0.58.

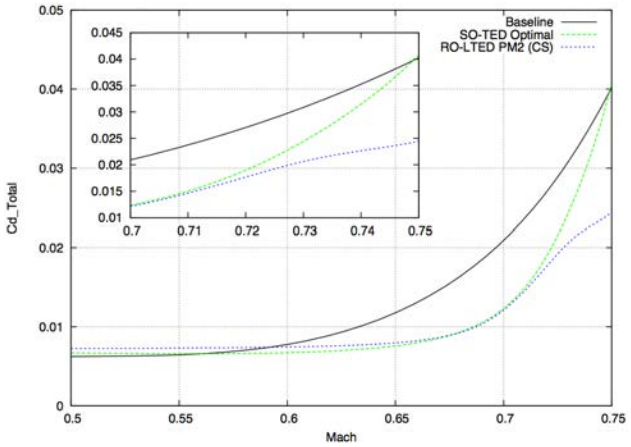

Fig. 16. Cd_{Total} vs. M_∞ sweep obtained by the baseline design and the optimal morphing configuration at Mach number range of [0.5:0.75] with $\mu Cl = 0.5558$, Re = 19.0×10^6 and $\mu x_{tr} = 25.65\%c$.

5 Conclusion

In this paper, a robust evolutionary optimisation technique was applied to the morphing wing/aerofoil design optimisation. Analytical research shows the benefits of coupling an optimisation method with robust design techniques to produce stable and high performance solutions. The use of morphing technique; LTED on an existing aerofoil, can reduce significantly the transonic drag which will save operating and manufacturing cost as well as emission reduction. Future work will focus on robust design optimization of morphing method on a 3D wing.

References

[1] Skillen, M., Crossley, W., Modeling and optimization for morphing wing concept generation, NASA/CR-2007-2148 60, March 2007.

[2] Namgoog, H., Crossley, W.A., and Lyrintzis, A.S., Aerodynamic Optimization of a Morphing Airfoil using Energy as an Objective, AIAA Journal Vol. 45 (9) pp. 2113 – 2124. 2007.

[3] Finnish Database Workshop "Integrated Multiphysics Simulation & Design Optimization: An Open Database Workshop for Multiphysics Software Validation" (http://www.mit.jyu.fi/scoma/DBW2010/), Univ. of Jyvaskyla, Finland, March 2010.

[4] Taguchi, G., Chowdhury, S., *Robust Engineering*, McGraw–Hill, New York, 2000.

[5] Lee, D.S., Gonzalez L.F., Srinivas K., Periaux, J., *Robust Design Optimisation using Multi-Objective Evolutionary Algorithms*, An International Journal Computers and Fluids. Vol 37. Issue 5, pages 565-583, ISSN 0045-7930. 2008.

[6] Lee, D.S., Periaux, J., Gonzalez, L.F., Onate, E., Qin, N., Active Transonic Aerofoil Design Optimization Using Robust Multi-objective Evolutionary Algorithms. *AIAA - Journal of Aircraft*. DOI: 10.2514/1.C031237 (2011)

[7] Lee, D.S., Bugeda, G., Periaux, J., Onate, E., Robust Active Shock Control Bump Design Optimisation using Parallel Hybrid-Game. 23rd International Conference on Parallel Computational Fluid Dynamics, Barcelona Spain, May 16-20, 2011.

[8] Z. Michalewicz,, *Genetic Algorithms + Data Structures = Evolution Programs*. Artificial Intelligence, Springer-Verlag, 1992.

[9] K. Deb, Multi-Objective Optimization using Evolutionary Algorithms Wiley & Sons, 2001.

[10] J. Kennedy, and R. Eberhart, Particle Swarm Optimization, Proceeding of IEEE International Conference on Neural Networks. IV. pp. 1942 – 1948, 1995.

[11] R. van der Pas. An Overview of OpenMP 3.0, Tutorial - International Workshop on OpenMP 2009 (IWOMP), Dresden, German, June 3, 2009.

[12] M. Drela, *A User's Guide to MSES 2.95*. MIT Computational Aerospace Sciences Laboratory, September 1996.

[13] P.H. Cook, M.A. McDonald, M.C.P. Firmin, Aerofoil RAE 2822 – Pressure Distributions, and Boundary Layer and Wake Measurements, Experimental Data Base for Computer Program Assessment, AGARD Report AR 138, 1979.

Copyright Statement